第４部　患者家族会の要望　15：30～16：00　座長　山田　章子（小児神経伝達物質病家族会代表）

① AADC欠損症：山田章子(東京)

② SSADH欠損症：久保田正代（千葉）

③ メンケス病：田中智次（大阪）

第５部　総合討論　16：00～16：20　司会　新宅治夫（大阪市立大学医学部小児科学教授）

閉会の辞　一瀬　宏（東京工業大学大学院生命理工学研究科　教授）

平成23年度「厚生労働科学研究費補助金 難治性疾患克服研究事業」

テーマ

３班合同公開シンポジウム

「難病・希少疾患を理解し克服する」

２月 平成２４年

１９日(日)

午前11時～午後４時

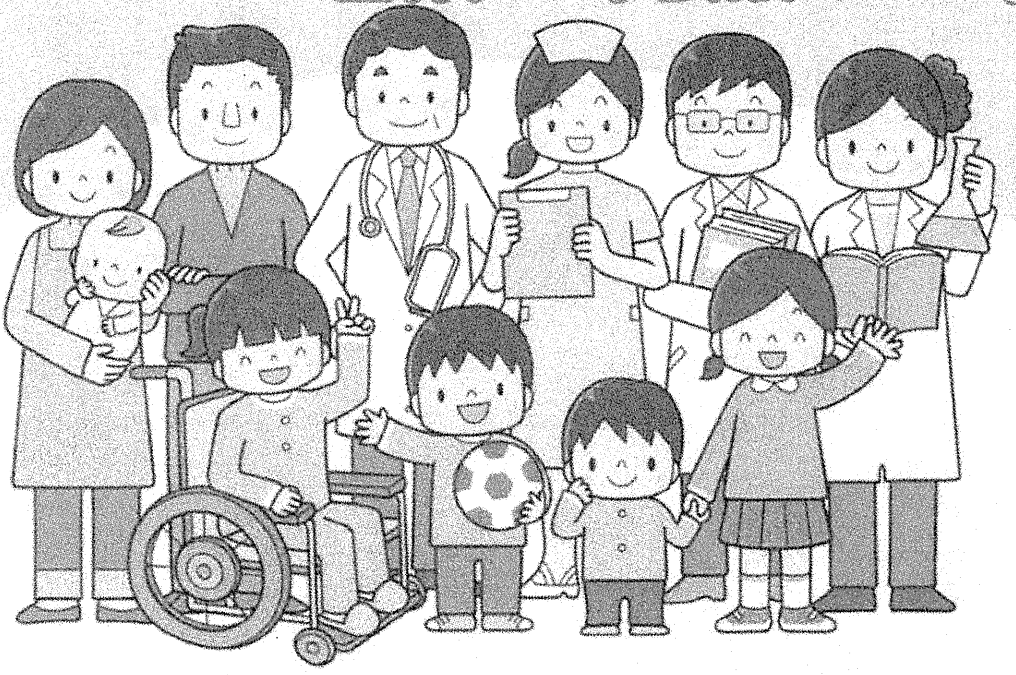

【会　場】 帝京大学講堂

本部棟４階・第１会議室

住所：東京都板橋区加賀２丁目１１－１

電話：03-3964-1211（代表）

内線651494（小児科遺伝代謝研究室）

【定　員】 100名

事前申込が必要です

下記宛てにメールでお申し込みください。

ｱﾄﾞﾚｽ:yuu1220@med.teikyo-u.ac.jp

【参加費】 無料

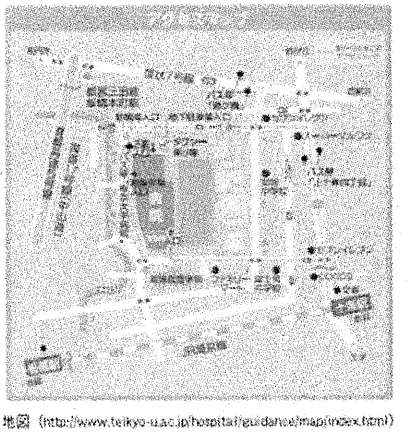

地図（http://www.teikyo-u.ac.jp/hospital/guidance/map/index.html）

【主催】

・Menkes 病・occipital horn 症候群の実態調査、早期診断基準確率、治療法開発（研究代表　帝京大学　客員教授 児玉浩子）

・小児神経伝達物質病の診断基準の作成と新しい治療法の開発に関する研究（研究代表　大阪市立大学　教授 新宅治夫）

・エカルディーグティエール症候群等のピオプテリン代謝異常を伴う疾患の診断方法確率および治療法開発のための横断的研究（研究代表　東京工業大学　教授 一瀬 宏）

平成23年度「厚生労働科学研究費補助金　難治性疾患克服研究事業」

3班合同公開シンポジウム「難病・希少疾患を理解し克服する」

【テーマ】難病・希少疾患の理解と克服

（1）Menkes 病・occipital horn 症候群の調査、診断と治療
（2）小児神経伝達物質病の診断と治療
（3）遺伝性ジストニアなどビオプテリン代謝異常を伴う疾患の診断と治療
（4）難病・希少疾患の家族からの要望

11:00 開場

11:05 **開会の辞：児玉浩子（帝京大学医学部小児科）**

第1部

児玉班
座長：児玉浩子（帝京大学医学部小児科）
① micro PET を用いたメンケス病モデルマウスにおける銅キレート剤の効果に関する研究
演者：野村志保（大阪市立大学医学部小児科）
② Menkes 病患者皮膚線維芽細胞を用いた分泌銅酵素 Lysyl Oxidase (LOX) 活性に対する Diethyldithiocarbamate (DEDTC) の効果の検討
演者：廣木伴子（帝京大学医学部小児科）
③ Menkes 病患者の早期発見に関する研究
演者：顧艶紅（成育医療研究センター研究所）
④ メンケス病・Occipital Horn 症候群におけるジスルフィラムの治療効果について
演者：小川英伸（帝京大学医学部小児科）

12:05 **昼　食**

13:05 **第2部**

新宅班
座長：新宅治夫（大阪市立大学医学部小児科）
① 小児神経伝達物質病の現状と今後の展望
「疾患概念の周知と新しい診断・治療法の開発を目指して」
演者：新宅治夫（大阪市立大学大学医学部小児科）
② ドーパ反応性ジストニア（DRD）とパーキンソン病（PD）の違い
「DRD に関与する黒質線条体ドーパミンニューロンは PD にかかわる黒質線条体ドーパミンニューロンとは異なる。」
演者：瀬川昌也（瀬川小児神経クリニック）
③ AADC 欠損症におけるメラトニン代謝
「唾液中メラトニン濃度測定による AADC 欠損症スクリーニング検査の可能性について」
演者：井手秀平（東京都立東部療育センター小児科）
④ SSADH 欠損症の臨床像と病態生理
「SSADH 欠損症の病態と診断について－自験2症例を中心に－」
演者：梶田光春（豊田厚生病院小児科）

14:05

14:05 **第3部**

一瀬班
座長：一瀬　宏
（東京工業大学大学院生命理工学研究科）
① 線条体におけるドーパミン生合成調節機構について
演者：徳岡宏文（東京工業大学大学院生命理工学研究科）
② 本邦における Aicardi-Goutières 症候群・famililal chilblain lupus の遺伝子異常について
演者：阿部純也、西小森隆太、井澤和司、河合朋樹、八角高裕、平家俊男（京都大学小児科）

14:35 **休憩**

14:50 **第4部**

患者家族会の要望
座長：山田章子
（小児神経伝達物質病家族会　代表）
メンケス病：田中智次（大阪）
AADC 欠損症：山田章子（東京）
SSADH 欠損症：久保田正代（千葉）

15:20 **第5部**

総合討論
司会　新宅治夫
（大阪市立大学医学部小児科）

15:50 **閉会**

16:00 **閉会の辞：一瀬　宏**
（東京工業大学大学院生命理工学部研究科）

memo

［資料５］

エカルディ - グティエール症候群
(Aicardi-Goutières syndrome; AGS)

１．概要

遺伝的に複合的な常染色体劣性遺伝性の疾患である。家族性の幼児期に見られる脳症で、脳内石灰沈着と髄液細胞数上昇があり、偽先天性トキソプラズマ脳症 あるいは偽 TORCH 症候群とも呼ばれる。

２．疫学

国内でおよそ数十名

３．原因

これまでに、原因遺伝子別に 5 つのサブグループ（AGS1-AGS5）に分類されている。AGS 1 は TREX1 遺伝子（3p21.3-p21.2）変異による。AGS2 は RNASEH2B 遺伝子（13q）、AGS3 は RNASEH2C 遺伝子（11q13.2）、AGS4 は RNASEH2A 遺伝子（19p13.13）、 AGS5 は SAMHD1 遺伝子（第 20 染色体）の変異によっておこる。同じ変異で優性遺伝となることもある。TREX1 変異が最も重症型になる。

４．症状

胎生期ウイルス感染様の表現形をとる。乳児期に重篤な神経症状を示し、進行性の小頭症、痙縮、ジストニア姿勢、高度の精神発達遅滞がみられ、小児期早期に死亡する。画像では脳萎縮、白質ジストロフィー、頭蓋内石灰化（基底核その他）があり、検査では慢性的な髄液リンパ球増多、髄液中のインターフェロンαとネオプテリンの増加がみられる。感染指標には異常がない。

５．合併症

神経系外の合併症としては血小板減少症、肝脾腫、肝酵素上昇、間歇的発熱がみられ、感染症を思わせる。免疫異常を生じることもあり、皮疹を生じ全身性エリテマトーデス(SLE)様となることもある。補体が減少し IgG と IgM は上昇する。非神経症状として凍瘡が 4 割の患者に認められている。

６．治療法

対症療法にとどまる。

［資料６］

ドーパ反応性ジストニア（瀬川病を含む）

1. 概要

14q22.1-22.2に存在するGTPシクロヒドロラーゼ１の変異により発症する常染色体優性遺伝性疾患である。筋緊張異常によるジストニアを主徴とする。10歳以下の発症が多く、女性に多い。成人発症例もある。常染色体劣性型もありチロシン水酸化酵素遺伝子の変異による。

2. 疫学

国内に数百名の瀬川病患者がいると考えられる。チロシン水酸化酵素遺伝子の変異による患者は、我が国ではまだ見つかっていない。

3. 原因

1994年に本疾患の原因遺伝子が、GTPシクロヒドロラーゼⅠ遺伝子であることが解明された。GTPシクロヒドロラーゼⅠは、ドーパミンの産生に必須なテトラヒドロビオプテリンの生合成酵素であり、患者では一対の本酵素遺伝子の片方に変異を有するために十分量のテトラヒドロビオプテリンを生合成することができず、結果として脳内でのドーパミン量が不足するためにジストニア症状を発症する。

4. 症状

下肢ジストニアにより歩行障害をきたす。尖足、内反尖足が多い。日内変動があり、昼から夕方にかけて症状が悪化し、睡眠によって改善する。固縮、姿勢時振戦がある。レボドパにより著明に改善する。成人発症例では、パーキンソン病様症状などで発症する例も報告されている。

5. 合併症

知能発達に異常は認められず、脳の器質的病変も伴わない。

6. 治療法

L-ドーパの投与が著効する。パーキンソン病患者にみられるようなL-ドーパ長期服用による副作用も発現しない。

[II] 研究成果の刊行に関する一覧表

研究成果の刊行に関する一覧表

雑誌

発表者氏名	論文タイトル名	発表誌名	巻	ページ	出版年
Nambu A	GABA-B receptor: possible target for Parkinson's disease therapy.	Exp Neurol	233	121-122	2012
Tokuoka H, Muramatsu S, Sumi-Ichinose C, Sakane H, Kojima M, Aso Y, Nomura T, Metzger D, Ichinose H	Compensatory regulation of dopamine after ablation of the tyrosine hydroxylase gene in the nigrostriatal projection.	J Biol Chem	286	43549-43558	2011
Nishibayashi H, Nambu A, Tachibana Y, Itakura T	Re: Cortically evoked responses of human pallidal neurons.	Mov Disord	26	2583-2584	2011
Tachibana Y, Iwamuro H, Kita H, Takada M, Nambu A	Subthalamo- pallidal interactions underlying parkinsonian neuronal oscillations in the primate basal ganglia.	Eur J Neurosci	34	1470-1484	2011
Takara S, Hatanaka N, Takada M, Nambu A	Differential activity patterns of putaminal neurons with inputs from the primary motor cortex and supplementary motor area in behaving monkeys.	Journal of Neurophysiol	106	1203-1217	2011
Yumoto N, Lu X, Henry TR, Miyachi S, Nambu A, Fukai T, Takada M	A neural correlate of the processing of multi-second time intervals in primate prefrontal cortex.	PLoS ONE	6(4)	e19168	2011
Nambu A	Somatotopic organization of the primate basal ganglia.	Front Neuroanat	5	26	2011
Nambu A, Chiken S, Shashidharan P, Nishibayashi H, Ogura M, Kakishita K, Tanaka S, Tachibana Y, Kita H, Itakura T	Reduced pallidal output causes dystonia.	Front Sys Neurosci	5	89	2011
Yasuda T, Hayakawa H, Nihira T, Ren Y-R, Nagai M, Hattori N, Miyake K, Takada M, Shimada T, Mizuno Y, Mochizuki, H	Parkin-mediated dopaminergic neuroprotection in an MPTP-minipump mouse model of Parkinson's disease.	J Neuropath Exp Neurol	70	686-697	2011

Masuda M, Miura M, Inoue R, Imanishi M, Saino-Saito S, Takada M, Kobayashi K, Aosaki T	Postnatal development of tyrosine hydroxylase mRNA-expressing neurons in mouse neostriatum.	Eur J Neurosci	34	1355-1367	2011
南部　篤	気になる脳部位　視床下核.	分子精神医学	11	203-206	2011
Koshiba S, Tokuoka H, Yokoyama T, Horiuchi E, Ichinose H, Hasegawa K	Biopterin levels in the cerebrospinal fluid of patience with PARK8 (I2020T)	J Neural Transm	118	899-903	2011
D. Homma, C. Sumi-Ichinose, H. Tokuoka, K. Ikemoto, Y. Nomura, K. Kondo, S. Katoh and H. Ichinose.	Partial Biopterin Deficiency Disturbs Postnatal Development of the Dopaminergic System in the Brain	J Biol Chem	286	1445-1452	2011
Nishibayashi H, Ogura M, Kakishita K, Tanaka S, Tachibana Y, Nambu A, Kita K, Itakura T	Cortically evoked responses of human pallidal neurons recorded during stereotactic neurosurgery.	Mov Disord	26	469-476	2011
Saga Y, Hirata Y, Takahara D, Inoue K, Miyachi S, Nambu A, Tanji J, Takada M, Hoshi E	Origins of multisynaptic projections from the basal ganglia to rostrocaudally distinct sectors of the dorsal premotor area in macaques.	Eur J Neurosci	33	285-297	2011
Hashimoto M, Takahara D, Hirata Y, Inoue K, Miyachi S, Nambu A, Tanji J, Takada M, Hoshi E	Motor and non-motor projections from the cerebellum to rostrocaudally distinct sectors of the dorsal premotor cortex in macaques.	Eur J Neurosci	31	1402-1413	2010
Kubo M, Kamiya Y, Nagashima R, Maekawa T, Eshima K, Ohta E, Obata F	LRRK2 is expressed in B-2 but not in B-1 B cells, and downregulated by cellular activation.	J Neuro-Immunol	229	123-128	2010
Ohta E, Kubo M, Obata F	Prevention of intracellular degradation of I2020T mutant LRRK2 restores its protectivity against apoptosis.	Biochem Biophys Res Commun	391	242-247	2010
Maekawa T, Kubo M, Yokoyama I, Ohta E, Obata F	Age-dependent and cell-population-restricted LRRK2 expression in normal mouse spleen.	Biochem Biophys Res Commun	392	431-435	2010
Sumi-Ichinose C, Ichinose H, Ikemoto K, Nomura T, Kondo K	Regulation of dopaminergic neural transmission by tyrosine hydroxylase protein at nerve terminals.	J. Pharmacol. Sci.	114	17-24	2010
南部　篤	臨床に役立つ大脳基底核の解剖と生理.	神経治療学	28	19-23	2011
南部　篤	線条体における運動手続き記憶.	Clinical Neuroscience	29	172-176	2011
平田幸一、長谷川一子、渡邊雅彦、Claudia Trenkwalder	レストレスレッグス症候群の鑑別診断と治療	日本医学会雑誌	138	RLS13-16	2010

長谷川一子	パーキンソン病治療の動向	最新医学	65	861-870	2010
長谷川一子	Huntington 病統一スケール（UHDRS)	神経内科	73	597-605	2010
長谷川一子	ジストニアとは	Clinical Meuroscience 別冊	28	742-745	2010
水野美邦、山本光利、久野貞子、長谷川一子、服部信孝	パーキンソン病治療における徐放性製剤の意義	新薬と臨牀	59	1820-1833	2010
長谷川一子	パーキンソン病の臨床診断および鑑別診断　−臨床症状から	綜合臨牀	59	2404-2411	2010

[III] 研究成果の刊行物・別刷

Experimental Neurology 233 (2012) 121–122

Contents lists available at SciVerse ScienceDirect

Experimental Neurology

journal homepage: www.elsevier.com/locate/yexnr

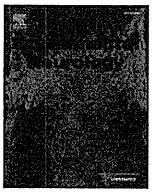

Commentary

GABA-B receptor: Possible target for Parkinson's disease therapy

Atsushi Nambu*

Division of System Neurophysiology, National Institute for Physiological Sciences and Department of Physiological Sciences, The Graduate University for Advanced Studies, Myodaiji, Okazaki 444-8585, Japan

In the recent issue of Experimental Neurology, Galvan et al. (2011) investigated the anatomical and physiological changes of γ-aminobutyric acid type B (GABA-B) receptors in the basal ganglia of parkinsonian monkeys. The basal ganglia play a key role in controlling voluntary movements, and their malfunctions cause movement disorders, such as Parkinson's disease and dystonia. The basal ganglia are composed of the striatum, subthalamic nucleus (STN), external (GPe) and internal (GPi) segments of the globus pallidus, and pars reticulata (SNr) and pars compacta (SNc) of the substantia nigra. Among these nuclei, the striatum is an input station of the basal ganglia, while the GPi and SNr are output nuclei. Two major pathways of the basal ganglia connect input and output structures: the striato-GPi/SNr direct and striato-GPe–STN–GPi/SNr indirect pathways (Albin et al., 1989; DeLong, 1990). GPe, GPi and SNr neurons receive GABAergic inputs from the striatum and GPe (GPe neurons receive GPe inputs through local axon collaterals of GPe neurons) and glutamatergic inputs from the STN (Boyes and Bolam, 2007; Nambu, 2007).

In order to understand normal functions of the basal ganglia and pathophysiology of movement disorders, it is essential to investigate how GABA is synthesized and released from synaptic terminals, binds to GABA receptors and is finally taken up by GABA transporters. GABA receptors are classified into ionotropic GABA-A and metabotropic GABA-B receptors. GABA-A receptors are responsible for fast inhibitory synaptic transmission. On the other hand, GABA-B receptors are responsible for slow and prolonged inhibitory transmission that may modulate firing rates and firing patterns of neurons. GABA-B receptors are heterodimers made up of GABA-BR1 and GABA-BR2 subunits. GABA-B receptors are located at both presynaptic and postsynaptic sites, and associated not only with GABAergic terminals from the striatum and GPe, but also with glutamatergic terminals from the STN (Boyes and Bolam, 2007; Nambu, 2007). A higher proportion of GABA-B receptors are located at extrasynaptic sites. Activation of the presynaptic GABA-B receptors inhibits transmitter (GABA and glutamate) release through a decrease in membrane Ca^{2+} conductance, whereas activation of postsynaptic GABA-B receptors induces an increase in membrane conductance through G protein-coupled inwardly-rectifying potassium channels (GIRK or Kir3) (Emson, 2007).

Parkinson's disease is caused by loss of dopaminergic neurons in the SNc and is characterized by tremor at rest, akinesia (poverty and slowness of movements) and muscle rigidity. In addition to these classical motor symptoms, nondopaminergic and/or nonmotor symptoms, such as loss of postural reflexes, bradyphrenia (slowness in mental function), depression, sleep disturbances, sensory complaints and autonomic disturbances occur. So far, there are two major models explaining pathophysiology underlying the motor symptoms of Parkinson's disease: the firing rate model vs. firing pattern model (Nambu, 2008). Dopamine depletion decreases the activity of striatal direct pathway neurons and increases the activity of striatal indirect pathway neurons. The firing rate model proposes that activity imbalance between the direct and indirect pathways induces an increase in the mean firing rate of GPi/SNr neurons (DeLong, 1990). Increased GABAergic outputs from the GPi/SNr suppress thalamo-cortical activity, resulting in akinesia. However, recent electrophysiological studies using parkinsonian monkeys have not always detected such an increase in GPi activity (Nambu, 2008). On the other hand, unit activity and local field potentials recorded from the GPe, GPi, SNr and STN of parkinsonian patients and animals showed oscillatory, synchronized and/or bursting activity. The firing pattern model proposes that these abnormal firing patterns disturb information processing through the basal ganglia (Bergman et al., 1998).

In addition, GABAergic neurotransmission itself within the basal ganglia may be altered in Parkinson's disease. It was reported that mRNA levels of the GABA-synthesizing enzyme, glutamate decarboxylase (GAD67 and GAD65), were increased in striato-GPe, GPi and SNr neurons (Pedneault and Soghomonian, 1994; Soghomonian and Laprade, 1997; Soghomonian et al., 1994). In the GPe, mRNA levels of GAD67, not GAD65 (Pedneault and Soghomonian, 1994; Soghomonian and Chesselet, 1992; Soghomonian et al., 1994), and GABA levels examined by in vivo microdialysis (Bianchi et al., 2003) were increased. The expression levels of GABA-A and GABA-B receptors were changed as well. GABA-A receptor binding and mRNA levels were decreased in the GPe and increased in the GPi/SNr of parkinsonian patients and animals (Calon et al., 1995, 2003; Chadha et al., 2000; Gnanalingham and Robertson, 1993; Katz et al., 2005). Similarly, GABA-B receptor levels were decreased in the GPe and increased in the GPi/SNr (Calon et al., 2000, 2003; Johnston and Duty, 2003). GABA-B receptor changes may be attributable to changes in GABA-BR1 mRNA expression. The GABA-A and GABA-B receptor changes observed in the GPe and GPi/SNr seem to be compensatory responses for the hyperactive striato-GPe indirect pathway and hypoactive striato-GPi direct pathway. Levodopa or dopaminergic agonists partially reversed the changes of GABA-A

☆ Commentary to Galvan, A., Hu, X., Smith, Y., Wichmann, T., 2011. Localization and pharmacological modulation of GABA-B receptors in the globus pallidus of parkinsonian monkeys. Exp. Neurol. 229: 429–439.

* Fax: +81 564 52 7913.
E-mail address: nambu@nips.ac.jp.

0014-4886/$ – see front matter
doi:10.1016/j.expneurol.2011.10.012

receptors in the GPe (Calon et al., 1995) and SNr/GPi (Calon et al., 1999; Gnanalingham and Robertson, 1993; Katz et al., 2005) and the changes of GABA-B receptors in the GPi (Calon et al., 2000). Parkinsonian patients and animals with higher levels of GABA-A or GABA-B receptors in the GPi had a tendency to exhibit dyskinesia with chronic dopamine treatments (Calon et al., 1995, 2000, 2003). This may be because upregulation of GABA-A and/or GABA-B receptors in the GPi causes suppression of GABAergic outputs from the GPi to release enhanced thalamo-cortical activity, leading to involuntary movements such as dyskinesia (see Waszczak and Walters, 1984).

Although the above studies repeatedly reported the expression changes of GABA-B receptors in Parkinsonism, it has not been clarified yet whether such changes contribute to neuronal activity changes in the basal ganglia. Galvan et al. (2011) demonstrated that the effects of local microinjection of a GABA-B receptor agonist/antagonist on GPe/GPi activity significantly differed between normal and parkinsonian monkeys, despite the fact that cellular and ultrastructural localization of GABA-BR1 subunits in the GPe/GPi was not altered. The GABA-B receptor agonist decreased the firing rate of GPe/GPi neurons of both normal and parkinsonian monkeys, probably through postsynaptic effects, but the magnitude of reduction in GPe neurons was larger in parkinsonian monkeys. The GABA-B receptor antagonist did not significantly affect the activity of GPi neurons in normal monkeys, whereas it reduced the firing rate of GPi neurons in parkinsonian monkeys, probably through a blockade of presynaptic GABA-B receptors in the GABAergic terminals. In addition, the GABA-B receptor agonist into the GPe and GPi, and the GABA-B receptor antagonist into the GPi increased rebound bursts in parkinsonian animals, but not in normal monkeys. Thus, GABA-B receptor-mediated modulation of synaptic transmission is profoundly altered in parkinsonian monkeys, and may contribute to firing rate and firing pattern changes, especially bursting activity of GPe and GPi neurons in the parkinsonian state. The study by Galvan et al. (2011) suggests that the GABA-B receptor could become a possible new target for drug therapy in Parkinson's disease. Normalization of GABA-B receptor-mediated responses may provide beneficial effects on parkinsonian symptoms.

References

Albin, R.L., Young, A.B., Penney, J.B., 1989. The functional anatomy of basal ganglia disorders. Trends Neurosci. 12, 366–375.

Bergman, H., Feingold, A., Nini, A., Raz, A., Slovin, H., Abeles, M., Vaadia, E., 1998. Physiological aspects of information processing in the basal ganglia of normal and parkinsonian primates. Trends Neurosci. 21, 32–38.

Bianchi, L., Galeffi, F., Bolam, J.P., Della Corte, L., 2003. The effect of 6-hydroxydopamine lesions on the release of amino acids in the direct and indirect pathways of the basal ganglia: a dual microdialysis probe analysis. Eur. J. Neurosci. 18, 856–868.

Boyes, J., Bolam, J.P., 2007. Localization of GABA receptors in the basal ganglia. Prog. Brain Res. 160, 229–243.

Calon, F., Goulet, M., Blanchet, P.J., Martel, J.C., Piercey, M.F., Bédard, P.J., Di Paolo, T., 1995. Levodopa or D2 agonist induced dyskinesia in MPTP monkeys: correlation with changes in dopamine and $GABA_A$ receptors in the striatopallidal complex. Brain Res. 680, 43–52.

Calon, F., Morissette, M., Goulet, M., Grondin, R., Blanchet, P.J., Bédard, P.J., Di Paolo, T., 1999. Chronic D1 and D2 dopaminomimetic treatment of MPTP-denervated monkeys: effects on basal ganglia $GABA_A$/benzodiazepine receptor complex and GABA content. Neurochem. Int. 35, 81–91.

Calon, F., Morissette, M., Goulet, M., Grondin, R., Blanchet, P.J., Bédard, P.J., Di Paolo, T., 2000. ^{125}I-CGP 64213 binding to $GABA_B$ receptors in the brain of monkeys: effect of MPTP and dopaminomimetic treatments. Exp. Neurol. 163, 191–199.

Calon, F., Morissette, M., Rajput, A.H., Hornykiewicz, O., Bédard, P.J., Di Paolo, T., 2003. Changes of GABA receptors and dopamine turnover in the postmortem brains of parkinsonians with levodopa-induced motor complications. Mov. Disord. 18, 241–253.

Chadha, A., Dawson, L.G., Jenner, P.G., Duty, S., 2000. Effect of unilateral 6-hydroxydopamine lesions of the nigrostriatal pathway on $GABA_A$ receptor subunit gene expression in the rodent basal ganglia and thalamus. Neuroscience 95, 119–126.

DeLong, M.R., 1990. Primate models of movement disorders of basal ganglia origin. Trends Neurosci. 13, 281–285.

Emson, P.C., 2007. $GABA_B$ receptors: structure and function. Prog. Brain Res. 160, 43–57.

Galvan, A., Hu, X., Smith, Y., Wichmann, T., 2011. Localization and pharmacological modulation of GABA-B receptors in the globus pallidus of parkinsonian monkeys. Exp. Neurol. 229, 429–439.

Gnanalingham, K.K., Robertson, R.G., 1993. Chronic continuous and intermittent L-3,4-dihydroxyphenylalanine treatments differentially affect basal ganglia function in 6-hydroxydopamine lesioned rats—an autoradiographic study using [^{3}H]flunitrazepam. Neuroscience 57, 673–681.

Johnston, T., Duty, S., 2003. Changes in $GABA_B$ receptor mRNA expression in the rodent basal ganglia and thalamus following lesion of the nigrostriatal pathway. Neuroscience 120, 1027–1035.

Katz, J., Nielsen, K.M., Soghomonian, J.J., 2005. Comparative effects of acute or chronic administration of levodopa to 6-hydroxydopamine-lesioned rats on the expression of glutamic acid decarboxylase in the neostriatum and $GABA_A$ receptors subunits in the substantia nigra, pars reticulata. Neuroscience 132, 833–842.

Nambu, A., 2007. Globus pallidus internal segment. Prog. Brain Res. 160, 135–150.

Nambu, A., 2008. Seven problems on the basal ganglia. Curr. Opin. Neurobiol. 18, 595–604.

Pedneault, S., Soghomonian, J.J., 1994. Glutamate decarboxylase (GAD65) mRNA levels in the striatum and pallidum of MPTP-treated monkeys. Brain Res. Mol. Brain Res. 25, 351–354.

Soghomonian, J.J., Chesselet, M.F., 1992. Effects of nigrostriatal lesions on the levels of messenger RNAs encoding two isoforms of glutamate decarboxylase in the globus pallidus and entopeduncular nucleus of the rat. Synapse 11, 124–133.

Soghomonian, J.J., Laprade, N., 1997. Glutamate decarboxylase (GAD67 and GAD65) gene expression is increased in a subpopulation of neurons in the putamen of parkinsonian monkeys. Synapse 27, 122–132.

Soghomonian, J.J., Pedneault, S., Audet, G., Parent, A., 1994. Increased glutamate decarboxylase mRNA levels in the striatum and pallidum of MPTP-treated primates. J. Neurosci. 14, 6256–6265.

Waszczak, B.L., Walters, J.R., 1984. A physiological role for dopamine as modulator of GABA effects in substantia nigra: supersensitivity in 6-hydroxydopamine-lesioned rats. Eur. J. Pharmacol. 105, 369–373.

THE JOURNAL OF BIOLOGICAL CHEMISTRY VOL. 286, NO. 50, pp. 43549–43558, December 16, 2011

Compensatory Regulation of Dopamine after Ablation of the Tyrosine Hydroxylase Gene in the Nigrostriatal Projection*[S]

Received for publication, July 20, 2011, and in revised form, October 6, 2011 Published, JBC Papers in Press, October 25, 2011, DOI 10.1074/jbc.M111.284729

Hirofumi Tokuoka[‡1], Shin-ichi Muramatsu[§], Chiho Sumi-Ichinose[¶], Hiroaki Sakane[‡], Masayo Kojima[‡], Yoshinori Aso[‡], Takahide Nomura[¶], Daniel Metzger[‖‡‡], and Hiroshi Ichinose[‡2]**

*From the [‡]Department of Life Science, Graduate School of Bioscience and Biotechnology, Tokyo Institute of Technology, 4259 B-7, Nagatsuta, Midori-ku, Yokohama, 226-8501 Japan, the [§]Division of Neurology, Department of Medicine, Jichi Medical University, Tochigi 329-0498, Japan, the [¶]Department of Pharmacology, School of Medicine, Fujita Health University, Toyoake, Aichi 470-1192, Japan, the [‖]Institut de Génétique et de Biologie Moléculaire et Cellulaire, Illkirch F-67400, France, **CNRS, Illkirch, France, and the [‡‡]Université Louis Pasteur, Strasbourg F-67000, France*

Background: The tyrosine hydroxylase (TH) gene, essential for dopamine synthesis, is partially ablated in adult nigrostriatal projection.
Results: TH reduction in axon terminals is slower than in soma, and dopamine is better maintained than TH.
Conclusion: Striatal dopamine is compensatorily regulated by axonal TH level and L-DOPA synthesis activity per TH level.
Significance: This regulation has potential relevance to pathogenesis of Parkinson disease and other dopamine-related psychiatric disorders.

The tyrosine hydroxylase (TH; EC 1.14.16.2) is a rate-limiting enzyme in the dopamine synthesis and important for the central dopaminergic system, which controls voluntary movements and reward-dependent behaviors. Here, to further explore the regulatory mechanism of dopamine levels by TH in adult mouse brains, we employed a genetic method to inactivate the *Th* gene in the nigrostriatal projection using the Cre-*loxP* system. Stereotaxic injection of adeno-associated virus expressing Cre recombinase (AAV-Cre) into the substantia nigra pars compacta (SNc), where dopaminergic cell bodies locate, specifically inactivated the *Th* gene. Whereas the number of TH-expressing cells decreased to less than 40% in the SNc 2 weeks after the AAV-Cre injection, the striatal TH protein level decreased to 75%, 50%, and 39% at 2, 4, and 8 weeks, respectively, after the injection. Thus, unexpectedly, the reduction of TH protein in the striatum, where SNc dopaminergic axons innervate densely, was slower than in the SNc. Moreover, despite the essential requirement of TH for dopamine synthesis, the striatal dopamine contents were only moderately decreased, to 70% even 8 weeks after AAV-Cre injection. Concurrently, *in vivo* synthesis activity of L-dihydroxyphenylalanine, the dopamine precursor, per TH protein level was augmented, suggesting up-regulation of dopamine synthesis activity in the intact nigrostriatal axons. Collectively, our conditional *Th* gene targeting method demonstrates two regulatory mechanisms of TH in axon terminals for dopamine homeostasis *in vivo*: local regulation of TH protein amount independent of soma and trans-axonal regulation of apparent L-dihydroxyphenylalanine synthesis activity per TH protein.

The dopaminergic system is important for many brain functions, including voluntary movements (1) and reward-related behaviors (2). The dysfunction of dopaminergic transmission is involved in many neurological and psychiatric disorders, such as Parkinson disease (3), addiction (4), attention deficit hyperactive disorders (5), and schizophrenia (6). Although chronic alterations in the dopaminergic system may be relevant to these disorders, it is still unclear how the dopaminergic system is regulated over days to months. In Parkinson disease, motor symptoms exhibit only after a large loss of striatal dopamine (7), suggesting compensation for the loss of dopamine. Although studies on Parkinson disease have suggested multiple forms of compensatory mechanisms, including enhanced dopamine release and turnover (8, 9, 10, 11), it is not fully understood what cellular and molecular mechanisms underlie the long term regulation of striatal dopamine levels under non-degenerative conditions.

Chronic intervention in the dopamine system has been performed for many years by pharmacological methods although they exhibit limitations related to dose dependence, drug metabolism, and circuit specificity. Gene-targeting methods, including germ line knock-out mice (12–14) and dopamine-deficient mice (15–17), have been generated, but because dopaminergic transmissions are blocked from the early stage of brain development, these methods may induce developmental effects. To explore the regulatory mechanisms of the nigrostriatal dopaminergic system in the adult brain, we generated mice in which dopamine synthesis can be selectively abrogated in a spatio-temporally controlled manner. The nigrostriatal projection is the largest dopaminergic projection in the brain, and the dense dopaminergic axon terminals in the striatum are readily

* This work was supported by Grants-in-aid for Human Frontier Science Program; by Research Grant 18A-2 for Nervous and Mental Disorders from the Ministry of Health, Labor and Welfare of Japan; by KAKENHI from MEXT; by the Nakajima Foundation; and by Core Research for Evolutional Science and Technology, Japan Science and Technology Agency (CREST, JST).
[S] The on-line version of this article (available at http://www.jbc.org) contains supplemental Figs. 1–5.
[1] To whom correspondence may be addressed. Tel.: 81-45-924-5822; Fax: 81-45-924-5807; E-mail: htokuoka@bio.titech.ac.jp.
[2] To whom correspondence may be addressed. Tel.: 81-45-924-5822; Fax: 81-45-924-5807; E-mail: hichinos@bio.titech.ac.jp.

investigated in isolation from their cell bodies and dendrites. Because tyrosine hydroxylase (TH)[3] is the rate-limiting enzyme in dopamine biosynthesis (18), we generated transgenic mice that contain two *loxP* sites flanking the major coding exons of the *TH* gene (floxed *Th* mice).

A microinjection of adeno-associated viral (AAV) vector expressing Cre recombinase (AAV-Cre) (19, 20) into the substantia nigra pars compacta (SNc) of the floxed *Th* mice disrupted the expression of the *Th* gene in a subset of neurons in the SNc of the adult mice. Our biochemical and histochemical analyses suggest two regulatory mechanisms of axonal TH for dopamine homeostasis in the nigrostriatal projection. First, the TH protein level in axon terminals is regulated differently from that in soma. Second, *in vivo* apparent L-DOPA synthesis activity per TH protein level in a given axon is influenced by dopamine synthesis in the neighboring axons, which we propose as trans-axonal regulation of dopamine levels.

EXPERIMENTAL PROCEDURES

Production of Th Floxed Mice, Genotyping—To construct the targeting vector for generating a floxed *Th* allele, a 9.5-kb XhoI-EcoRI genomic DNA segment containing genomic *Th* DNA was isolated from a λ phage 129SV mouse genomic library. The EcoRI site located at the 3′-end was replaced by MluI, a HindIII restriction site was engineered by site-directed mutagenesis between exons 5 and 6, and the SpeI site located between exons 9 and 10 was converted into a NotI site. A *loxP* site and an EcoRV restriction site were inserted into a HindIII site, and a neomycin-resistant cassette, flanked by *loxP* sites, was inserted into a NotI site. The three *loxP* sites in the final targeting vector were in the same orientation (3′ to 5′) (Fig. 1*A*).

Mouse embryonic stem cells were electroporated with the targeting vector, and the homologously recombinated clones were screened by PCR and Southern blot analysis. Embryonic stem clones with three *loxP* sites were selected, and a plasmid expressing Cre DNA recombinase was transiently transfected into the cells. Embryonic stem cells with two *loxP* sites without a neomycin cassette were selected by PCR and used for production of chimeric mice.

The genotypes of mice were identified on mouse ear biopsies by PCR (30 cycles at 94 °C for 30 s, 65 °C for 3 min, and a final extension at 72 °C for 5 min) with primers TH9F (5′-CATTTGCCCAGTTCTCCCAG-3′) and TH10R (5′-AGAGATGCAAGTCCAATGTC-3′). The sizes of the PCR products amplified from the wild-type *Th* allele and from the floxed *Th* allele are 431 and 513 bp, respectively.

For the detection of recombined *Th* alleles, genomic DNA was extracted from the substantia nigra regions of brain slices fixed by paraformaldehyde. The recombined *Th* alleles were detected by PCR (30 cycles at 94 °C for 30 s, 66 °C for 30 s, 72 °C for 1 min 15 s, and a final extension at 72 °C for 5 min) with primers TH5F (5′-AGGCGTATCGCCAGCGCC-3′) and TH10Rb (5′-CCCCAGAGATGCAAGTCCAATGTC-3′). The sizes of the PCR products amplified from the wild-type *Th* allele, floxed *Th* allele, and deleted *Th* allele are 1722, 1886, and 430 bp, respectively.

AAV Vector Construction—We generated two types of AAV-Cre vectors basically as described previously (19). One was the AAV-Cre vector, which contained an expression cassette with a human cytomegalovirus immediate early promoter (CMV promoter), followed by the first intron of human growth hormone, Cre recombinase cDNA, and simian virus 40 polyadenylation signal sequence (SV40 poly(A)), between the inverted terminal repeats of the AAV-2 genome. The other was the AAV-GFP/Cre vector, which contained an expression cassette with a synapsin I promoter (21), followed by AcGFP1 (Clontech), the internal ribosomal entry site, Cre recombinase cDNA, and simian virus 40 polyadenylation signal sequence (SV40 poly(A)), between the inverted terminal repeats of the AAV-1 genome. The two helper plasmids, pHLP19 and pladeno1 (Avigen, Alameda, CA), harbored the AAV *rep* and *cap* genes as well as the E2A, E4, and VA RNA genes of the adenovirus genome, respectively. HEK293 cells were co-transfected with the vector plasmid, pHLP19, and pladeno1 by the calcium phosphate precipitation method. The AAV vectors were then harvested and purified by two rounds of continuous iodoxale ultracentrifugations. Vector titers were determined by quantitative DNA dot-blot hybridization or by quantitative PCR of DNase I-treated vector stocks. We routinely obtained 10^{12} to 10^{13} vector genome copies/ml.

Animals and Stereotaxic Microinjections—Mice were acclimated to and maintained at 25 °C under a 12-h light/dark cycle (light on 08:00–20:00). All animal experiments were performed in accordance with the general guidelines of the Tokyo Institute of Technology. Unilateral injections into the SNc were performed on 12–16-week-old mice that were anesthetized with Nembutal (intraperitoneally) and mounted into a stereotaxic apparatus. The coordinates were 3.0 mm posterior from bregma, 1.0 mm lateral to midline, and 4.0 mm ventral from the dural surface. 1 μl of AAV-Cre or AAV-GFP/Cre (about 10^9 particles) was injected through an injection cannula (28-gauge) with a Hamilton microsyringe driven by a microdialysis pump at a rate of 0.2 μl/min. After microinjection, the injection cannula was left for 2 min before its withdrawal to reduce the efflux of injected liquid along the injection tract. When a cannula was blocked or leaked, the mouse was excluded from the following experiments. The mice were sacrificed at 1, 2, 4, 8, or 16 weeks after microinjection for analyses. We used the uninjected side of a brain as a control side to compare with. $Th^{+/+}$ mice were used as control animals.

Immunohistochemistry—Striatal slices were prepared by transcardial perfusion with saline, followed by 4% paraformaldehyde, 60 mM phosphate buffer, and postfixation overnight. All solutions were used at 4 °C. In some experiments, striatal tissues were dissected and homogenized for Western blot and monoamine assay (see below), and the rest of the brain, including the midbrain with the SNc region, was fixed by immersing in 4% paraformaldehyde, PBS overnight. The fixed brain pieces

[3] The abbreviations used are: TH, tyrosine hydroxylase; AADC, aromatic L-amino acid decarboxylase; AAV, adeno-associated virus; AAV-Cre, adeno-associated virus expressing Cre recombinase; DA, dopamine; DAT, dopamine transporter; DOPAC, 3,4-dihydroxyphenylacetic acid; HVA, homovanillic acid; L-DOPA, L-dihydroxyphenylalanine; vMAT2, vesicular monoamine transporter 2; SNc, substantia nigra pars compacta; 6-OHDA, 6-hydroxydopamine; GBR12909, 1-[2-[bis-(4-fluorophenyl)methoxy]ethyl]-4-(3-phenylpropyl)piperazine dihydrochloride.

were cryoprotected by 30% sucrose, and the coronal slices of 30-μm thickness were cut by a cryostat. The free floating serial coronal sections, from the rostral to the caudal edge of SNc or a part of the striatum, were incubated with rabbit anti-TH antibody (1:10,000; Millipore) or rabbit anti-AADC serum (1:20,000) (12), followed by biotinylated goat anti-rabbit IgG antibody (1:250; Vector Laboratories) and avidin-peroxidase complex (Vectastain ABC kit, Vector Laboratories). Immunocomplexes were visualized by a reaction with 3,3′-diaminobenzidine tetrahydrochloride and 0.003% H_2O_2. Images were taken using an upright microscope (Eclipse E800, Nikon) equipped with a cooled CCD camera (VB-6010, Keyence).

The numbers of TH-positive neurons in the injected and uninjected side SNc were compared using a stereological cell counting method. SNc was defined according to the brain atlas (22). Briefly, one in every three coronal sections covering the whole SNc was selected (typically 12–14 sections) and stained for TH, and magnified images of SNc were taken using a 20× objective lens (numerical aperture 0.5). For each region of interest, images were taken at multiple different focus planes to visualize all cells in the thickness. The number of all TH-positive cells in SNc in each slice was counted manually with ImageJ (National Institutes of Health). Only cells with an apparently visible nucleus were included. The number of all TH-positive neurons from a set of slices was summed (typically 1600–2000 cells in the uninjected side), and the ratio of the number in the injected side to that in the uninjected side was evaluated.

For fluorescence immunohistochemistry, the following secondary antibodies were used: Alexa546-conjugated anti-mouse IgG (1:2,000; Invitrogen) and Alexa633-conjugated anti-rabbit IgG (1:2,000; Invitrogen). Images were taken using the TCS SPE confocal microscope (Leica) with a 63× oil objective lens and excitation lasers of 532 and 635 nm.

For the detection of dopamine, we fixed mice transcardially with 5% glutaraldehyde, and the brain sections made with vibratome were stained with rabbit anti-TH antibody or rabbit anti-dopamine-glutaraldehyde conjugate (1:500; Millipore). Because glutaraldehyde fixation induces very strong background fluorescence, we performed immunodetection with the avidin-peroxidase complex as described above instead of fluorescence detection.

Western Blotting—To dissect striatal tissues for biochemical assays, we first made a coronal section of 2-mm thickness from approximately +1.5 to 0.5 mm to the bregma using a brain matrix (Neuroscience, Inc., Tokyo). Then the left and right dorsal striata were dissected by a surgical blade under a stereo microscope and homogenized using the Pellet Mixer (TreffLab) in 150 μl of PBS containing 1 mM dithiothreitol, 2 mM EDTA, 2 mM NaF, 1 μg/ml leupeptin, 1 μg/ml pepstatin, 1 mM phenylmethylsulfonyl fluoride, and 0.1 mM pargyline, followed by centrifugation at 20,000 × *g* for 10 min at 4 °C. An aliquot of the supernatant was used for the monoamine assay. In some experiments, ventral midbrain homogenates were prepared similarly, except the positions of coronal sections were approximately −2.5 to −4.5 mm to the bregma. The striatal or ventral midbrain homogenates containing 10 μg of protein were separated by electrophoresis on a 10% SDS-polyacrylamide gel and transferred to a PVDF membrane. The membranes were immunodetected using the following primary antibodies: rabbit anti-TH antibody (1:10,000; Millipore), rabbit anti-AADC antibody (1:20,000) (12), or mouse anti-β-actin antibody (1:10,000; Sigma-Aldrich). Immunoreactive proteins were detected by peroxidase-conjugated secondary antibodies and Immobilon-Western (Millipore). Quantitative analyses were performed with LAS-3000 (Fujifilm).

For better quantification of low level TH proteins by Western blot, we assessed the linearity of the detection using serial dilution of striatal homogenates of the uninjected side (supplemental Fig. 1). Then we employed a range showing a linear relationship between actual loaded proteins (2.5–20 μg, or a 0.125–1.0 ratio) and measured TH protein levels (0.05–1 ratio). Within this range, we made a standard curve and calibrated the TH protein levels accordingly.

For detection of vesicular monoamine transporter 2 (vMAT2) and dopamine transporter (DAT) proteins, a crude synaptosomal fraction was prepared by homogenizing striatal tissues in 4 mM HEPES buffer containing 0.32 M sucrose, 2 mM NaF, 1 μg/ml leupeptin, 1 μg/ml pepstatin, 1 mM phenylmethylsulfonyl fluoride, and 0.1 mM pargyline. The homogenate was centrifuged at 900 × *g*, the supernatant was further centrifuged at 14,500 × *g*, and the resulting pellet (P2 fraction) was dissolved in 80 μl of the same HEPES buffer containing 1% SDS. Protein concentration was determined by the DC protein assay (Bio-Rad). 20 μg of each protein sample was analyzed by Western blot using the following primary antibodies: rabbit anti-vMAT2 antiserum (1:500; Synaptic Systems), rabbit anti-DAT antibody (1:500; Millipore), rabbit anti-TH antibody (1:10,000; Millipore), or mouse anti-β-actin antibody (1:10,000; Sigma-Aldrich).

For the detection of phospho-TH proteins, striatal homogenates were prepared by immediate boiling of a whole brain for 5 min after dissection, followed by isolation of striata and homogenization and sonication in 0.1 M Tris-HCl (pH 6.8) buffer containing 1% SDS. Protein concentration was determined by the DC protein assay (Bio-Rad). 60 μg of each protein sample was analyzed by Western blot using the following primary antibodies: rabbit anti-Ser(P)-40-TH antibody (1:2,000; Millipore), rabbit anti-p31-TH antibody (1:2,000; Millipore), or rabbit anti-TH antibody (1:10,000; Millipore).

Monoamine Assay—Aliquots of striatal supernatant were deproteinized by 60 mM perchloric acid with 30 μM EDTA and 30 μM pargyline on ice for 30 min and centrifuged at 20,000 × *g* for 15 min. The monoamine levels in the supernatant were analyzed by high performance liquid chromatography (HPLC) with an SC5-ODS column (EICOM) and a mobile phase buffer containing 84 mM acetic acid-citrate (pH 3.5), 5 μg/ml EDTA, 190 mg/ml sodium 1-octane sulfonate, and 16% methanol. Monoamines were detected by electrochemical detection (ECD-100, EICOM).

Biopterin contents were measured as described previously (43). Briefly, the deproteinized homogenates were oxidized by 0.1 M HCl containing 0.1% I_2 and 0.2% KI for 1 h at room temperature, followed by centrifugation at 20,000 × *g* for 10 min. The supernatants were neutralized by 0.2% ascorbic acid and then subjected to HPLC analyses with Inertsil ODS-3 column (GL Sciences) and a mobile phase buffer containing 10 mM

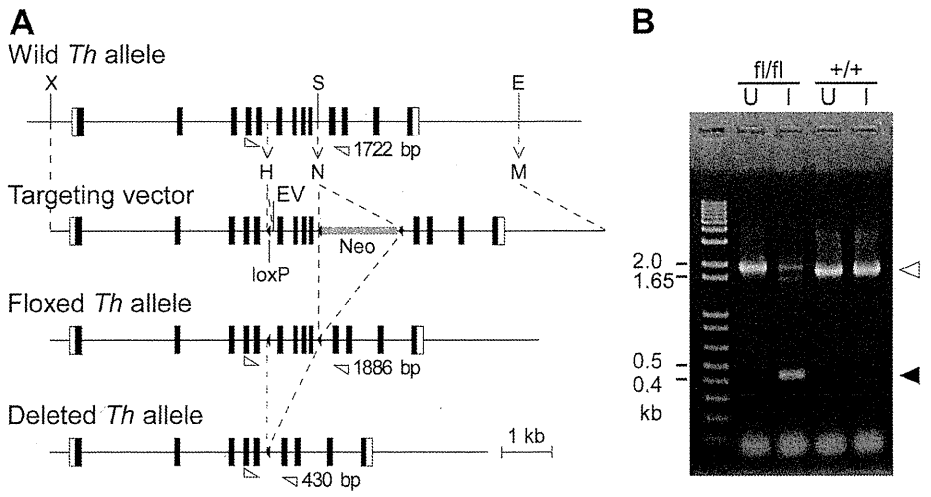

FIGURE 1. **Ablation of the *Th* gene by AAV-Cre injection into the SNc of the floxed *Th* mice.** *A*, schematic representation of the targeting vector for the generation of the floxed *Th* allele. *E*, EcoRI; *H*, HindIII; *M*, MluI; *N*, NotI; *S*, SpeI; *X*, XhoI; *Neo*, neomycin-resistant cassette. *Broken arrows* represent the generation or replacement of a restriction site. Exons are represented by *boxes*. The positions of the primers designed for the detection of genomic DNA recombination by PCR are indicated by *open triangles* with resulting PCR product sizes. *B*, PCR detection of genomic DNA recombination using primers for wild type (*open arrowhead*) or deleted *Th* (*closed arrowhead*) alleles. The template genomic DNA was prepared from the uninjected (*U*) or injected (*I*) side of the of the $Th^{fl/fl}$ or $Th^{+/+}$ mice 2 weeks after the unilateral microinjection of the AAV-Cre into the SNc. Note that the *Th* gene recombination was detected only in the injected side of the SNc of the $Th^{fl/fl}$ mice but not in the uninjected side of the $Th^{fl/fl}$ mice and the $Th^{+/+}$ mice.

$NaPO_4$ (pH 6.9) and a fluorescence detector (excitation 350 nm/emission 440 nm; RF-10A, Shimadzu, Tokyo).

Estimation of in Vivo L-DOPA Synthesis Activity per TH Protein Level—In vivo L-DOPA synthesis activity was evaluated by measuring the L-DOPA levels that accumulated in 30 min after the administration of 3-hydroxybenzylhydrazine dihydrochloride (NSD-1015, Sigma-Aldrich), an AADC inhibitor, to mice (100 mg/kg, intraperitoneal). The striatal tissues were homogenized using a pellet mixer (TreffLab) in 150 μl of PBS containing 1 mM dithiothreitol, 2 mM EDTA, 2 mM NaF, 1 μg/ml leupeptin, 1 μg/ml pepstatin, 1 mM phenylmethylsulfonyl fluoride, and 0.1 mM pargyline, followed by centrifugation at 20,000 $\times$ *g* for 10 min at 4 °C. An aliquot of the supernatant was used for assaying protein concentration by Bradford method, and Western blot to assess the TH protein levels. Another aliquot was deproteinized by 60 mM perchloric acid with 30 μM EDTA and 30 μM pargyline on ice for 30 min and centrifuged at 20,000 $\times$ *g* for 15 min. The supernatant was neutralized by K_2CO_3, and L-DOPA was purified by Al_2O_3 powder. The L-DOPA level was analyzed by HPLC with a NUCLEOSIL 100-7C18 reverse-phase column with a mobile phase buffer containing 0.1 M $NaPO_4$ (pH 3.5), 8 μM EDTA and electrochemical detection. To evaluate the *in vivo* L-DOPA synthesis activity per TH protein, L-DOPA accumulation was normalized to TH protein levels estimated by Western blot.

Rotation Test—Mice were placed in a round bowl (25 cm in diameter) for 20 min for acclimation. The mice were administered with 1-[2-[bis-(4-fluorophenyl)methoxy]ethyl]-4-(3-phenylpropyl)piperazine dihydrochloride (GBR12909; Tocris Bioscience; intraperitoneal, 30 mg/kg) and returned to the same bowl, and the behavior was videorecorded. The rotations were counted by visual observation for a 60-min period immediately after intraperitoneal injection. One rotation was defined by the animal completing a 360° turning without turning back in the opposite direction.

Statistics—The Mann-Whitney *U* test, Wilcoxon's signed rank test, or Steel's test was used as required. Spearman's rank correlation was used to evaluate a correlation between two groups. *p* values of <0.05 were considered significant. The data are shown as individual data points and mean values or as mean $\pm$ S.E., as indicated. Exponential and liner fittings were performed with Igor Pro 6.2 (WaveMetrics).

RESULTS

Production of Floxed Th Mice and Th Gene Ablation by AAV-Cre—First, we generated the floxed *Th* mice ($Th^{fl/fl}$) in which exons 6–9 of the *Th* gene were flanked by *loxP* sites (Fig. 1*A*). We used AAV-Cre to induce DNA recombination *in vivo* by performing a unilateral stereotaxic microinjection of the virus into the SNc of the adult floxed *Th* mice. Microinjection of AAV-Cre into the SNc induced DNA recombination in 2 weeks when we examined the substantia nigra tissue samples by PCR (Fig. 1*B*). *Th* gene recombination was detected in the injected side SNc of the $Th^{fl/fl}$ mice but not in the uninjected side of the $Th^{fl/fl}$ mice and both sides of the $Th^{+/+}$ mice. Thus, the floxed *Th* mice and AAV-Cre enabled us to induce *Th* gene ablation in the adult mouse midbrain.

Abrogation of TH Protein Expression in SNc Dopaminergic Neurons—Using immunohistochemistry, we next examined the effect of the AAV-Cre injection on TH protein expression in the SNc. The TH protein immunoreactivity was absent in the majority of neurons in the SNc 2 weeks after the AAV-Cre injection (Fig. 2*A* and *B*). We found that the number of TH-positive dopaminergic neurons normalized to the uninjected side was reduced by as early as 2 weeks, with the mean ratios of 38, 30, and 40% at 2, 4, and 8 weeks after the AAV-Cre injection, respectively, whereas they were unchanged in the $Th^{+/+}$ mice (97% at 8 weeks; Steel's test, $p = 0.0239$, 0.0166, and 0.0061 for the $Th^{fl/fl}$ mice at 2, 4, and 8 weeks, respectively, compared with the $Th^{+/+}$ at 8 weeks; Fig. 2*C*).

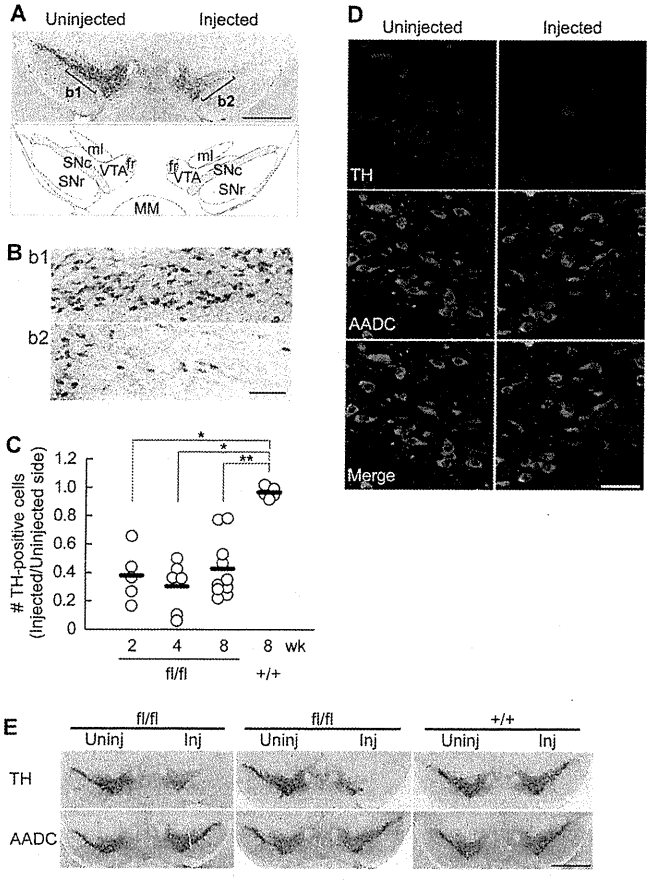

FIGURE 2. **AAV-Cre-induced loss of TH expression in the SNc.** *A*, a representative image of a midbrain slice immunostained for TH (*top*) and a schematic atlas (*bottom*). Serial coronal sections of the midbrains of the $Th^{fl/fl}$ mice were prepared 8 weeks after the AAV-Cre injection and were immunostained for TH. The SNc in the atlas is indicated by the *hatched area*. *fr*, fasciculus retroflexus; *ml*, medial lemniscus; *MM*, medial mammillary nucleus; *SNr*, substantia nigra pars reticulata; *VTA*, ventral tegmental area. *B*, magnified views of the uninjected side (*b1*) and injected side (*b2*) SNc as indicated in *A*. *C*, summary of the ratio of TH-positive cell numbers in the injected side SNc to the uninjected side. *Open circles* indicate the values from individual animals, and *bars* indicate the means. $n = 5$, 6, 11, and 5 brains for 2, 4, and 8 weeks ($Th^{fl/fl}$ mice) and 8 weeks ($Th^{+/+}$ mice) after injection, respectively. *, $p < 0.05$; **, $p < 0.01$, Steel's test. *D*, immunofluorescence staining for TH (*red*) and AADC (*green*) of the SNc of the $Th^{fl/fl}$ mice examined 2 weeks after the injection of AAV-GFP/Cre. TH and AADC were visualized with Alexa546 and Alexa633, respectively, distinguishing from GFP signal, and *pseudocolored* confocal images are shown. Note that the number of TH-expressing neurons was clearly reduced in the AAV-GFP/Cre-injected side, whereas the AADC, another dopaminergic neuron marker, remained expressed. *E*, TH deletion induces no apparent cell death in 16 weeks. Midbrain slices from two $Th^{fl/fl}$ mice and one $Th^{+/+}$ mouse were immunostained for TH and AADC 16 weeks after the AAV-Cre microinjection. Whereas the TH-expressing neurons were reduced in the injected side of the SNc of the $Th^{fl/fl}$ mice, the number of AADC-expressing neurons was apparently unaffected, suggesting that the dopaminergic neurons do not show cell death in the absence of TH in 16 weeks. *Scale bars*, 1 mm (*A*), 100 μm (*B*), 50 μm (*D*), and 1 mm (*E*).

To confirm a selective loss of TH protein, we also performed double immunofluorescence histochemistry for TH and aromatic AADC, a dopaminergic neuron marker. We used AAV-GFP/Cre for the purpose of labeling infected cells, but GFP expression in these neurons was too weak for detection, so we immunostained TH and AADC with Alexa546 and Alexa633 fluorophores, respectively, distinguishing from GFP signals. We found that the AADC immunoreactivity was preserved in the TH-negative neurons in the SNc 2 weeks after the AAV-GFP/Cre injection (Fig. 2*D*), suggesting that the AAV-GFP/Cre injection induced an efficient *Th* gene ablation without inducing cell death or damage. Moreover, AADC expression in the SNc was apparently unaffected in the $Th^{fl/fl}$ mice up to 16 weeks following the AAV-Cre injection, when the majority of the SNc dopaminergic neurons lost TH expression (Fig. 2*E*). These data suggest that dopamine is not essential for the survival of dopaminergic neurons in adult brains.

Slower Reduction of TH Proteins in Axon Terminals of Nigrostriatal Projection—The dopaminergic neurons in the SNc project their axons toward the striatum and form dense synapses (23, 24), where abundant TH proteins were contained. We quantitatively examined the reduction of the TH protein in the striatum by Western blot (Fig. 3*A* and *B*). The TH protein level was gradually reduced in the AAV-Cre injected side compared with the uninjected side in $Th^{fl/fl}$ mice, to 75, 50, and 39% at 2, 4, and 8 weeks after the AAV-Cre injection, respectively, whereas the levels were unchanged in the $Th^{+/+}$ mice (104% at 8 weeks; Steel's test, $p = 0.0932$, 0.0071, and 0.0059 for the $Th^{fl/fl}$ mice at 2, 4, and 8 weeks, respectively, compared with the $Th^{+/+}$ at 8 weeks; Fig. 3*B*). AADC protein levels did not show significant changes (Steel's test, $p = 0.77$, 0.92, and 0.88 for the $Th^{fl/fl}$ mice at 2, 4, and 8 weeks, respectively, compared with the $Th^{+/+}$ at 8 weeks; supplemental Fig. 2*A*).

We noticed that the reduction of TH protein level in the striatum could be slower than the reduction of the number of TH-expressing cells in the SNc because the difference between the two seemed remarkable at 2 weeks. To further investigate the difference, we compared the TH protein reductions in the striatum with that in ventral midbrain tissue, including SNc, using Western blot (Fig. 3*C*). We found that the TH protein reduction in the striatum showed a delay by about 2 weeks, whereas the decay time constants were similar ($\tau = 2.06$ and 2.04 weeks for the ventral midbrain and striatum, respectively).

We also used immunofluorescence histochemistry to examine the expression of TH and AADC in the striatum (Fig. 3*D*). Two weeks after the AAV-Cre injection, the number of TH-expressing axons in the injected side of the striatum of the $Th^{fl/fl}$ mice was only slightly reduced compared with the uninjected side, which was consistent with the Western blot data. However, the number of TH-expressing axons was decreased profoundly 8 weeks after the AAV-Cre injection. The number of AADC-expressing axons was apparently unchanged, suggesting that the axon terminals of the dopaminergic neurons remained mostly intact. These Western blot and immunohistochemical data indicate differential regulation of TH protein levels between axon terminals (striatum) and soma (SNc). Also, the *Th* gene ablation led to an almost complete and selective loss of TH protein in a subset of dopaminergic axons.

Better Maintenance of Striatal Dopamine Levels than TH Protein Levels—To investigate if dopamine levels follow the reduction of TH protein levels in the striatum, we assayed striatal monoamine contents using the same striatal extracts used in the Western blot analysis (Fig. 4*A*). The dopamine contents decreased gradually to around 98, 79, and 69% at 2, 4, and 8 weeks after the AAV-Cre injection, respectively, in the $Th^{fl/fl}$ mice but not in the $Th^{+/+}$ mice (104% at 8 weeks; Steel's test, $p = 0.98$, 0.0475, and 0.0637 for 2, 4, and 8 weeks in the $Th^{fl/fl}$

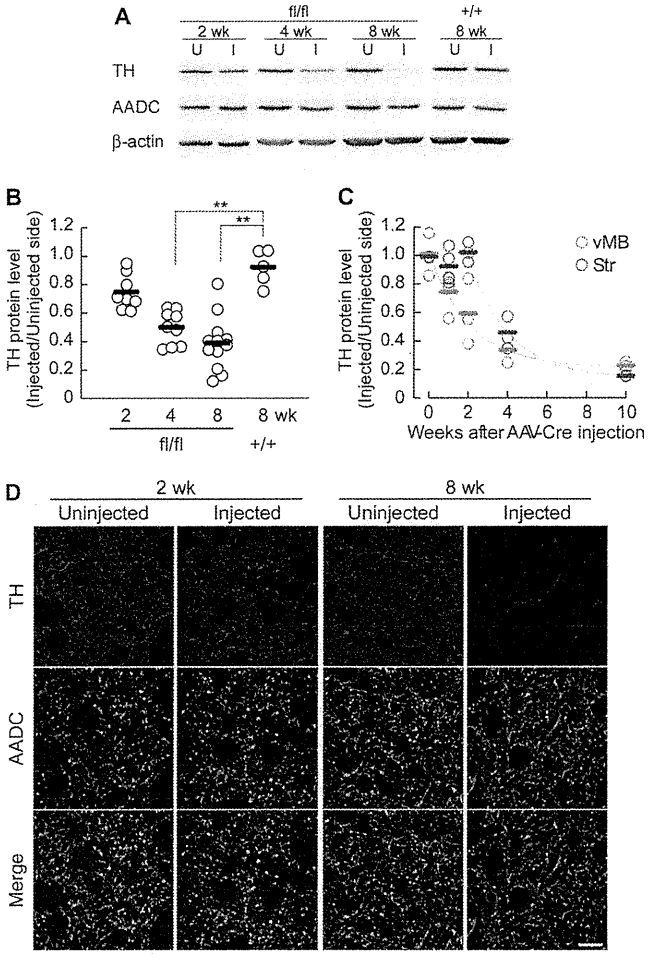

FIGURE 3. **Decrease in striatal TH protein levels after *Th* gene ablation.** *A*, striatal homogenates of each genotype were prepared 2, 4, or 8 weeks after the unilateral AAV-Cre injection into the SNc, and Western blot analysis was performed with antibodies against TH, AADC, and β-actin. *U* and *I*, uninjected and injected sides of the striatum, respectively. *B*, summarized quantitative analyses of Western blots for the striatal TH protein levels. The ratios of the protein level of the injected side to the uninjected side are plotted on the *vertical axis*. The *open circles* indicate the values from individual animals, and the *bars* indicate the means. n = 8, 9, 12, and 5 brains for 2, 4, and 8 weeks ($Th^{fl/fl}$ mice) and 8 weeks ($Th^{+/+}$ mice) after injection, respectively. *, $p < 0.05$; **, $p < 0.01$, Steel's test. *C*, comparison of TH protein levels in the striatum and ventral midbrain by Western blot. Tissue homogenates were prepared from the injected side and uninjected side of the ventral midbrain (*vMB*) and striatum (*Str*) of $Th^{fl/fl}$ mice and were subjected to Western blots for TH. n = 2, 4, 3, 2, and 3 for 0, 1, 2, 4, and 10 weeks after AAV-Cre injection, respectively. Data were fitted with an *exponential curve*. For the striatum, fitting was performed from 2 weeks because there was no apparent reduction before 2 weeks in this data set. *D*, decrease in the number of TH-expressing axons in the striatum. Striatal slices of the $Th^{fl/fl}$ mice were prepared 2 and 8 weeks after the injection of AAV-GFP/Cre and were immunohistochemically stained for TH (*red*) and AADC (*green*). TH and AADC were visualized as in Fig. 2*D*. *Merged images* are shown at the *bottom*. Images from the uninjected and injected side of the striatum are shown as indicated. *Scale bar*, 10 μm.

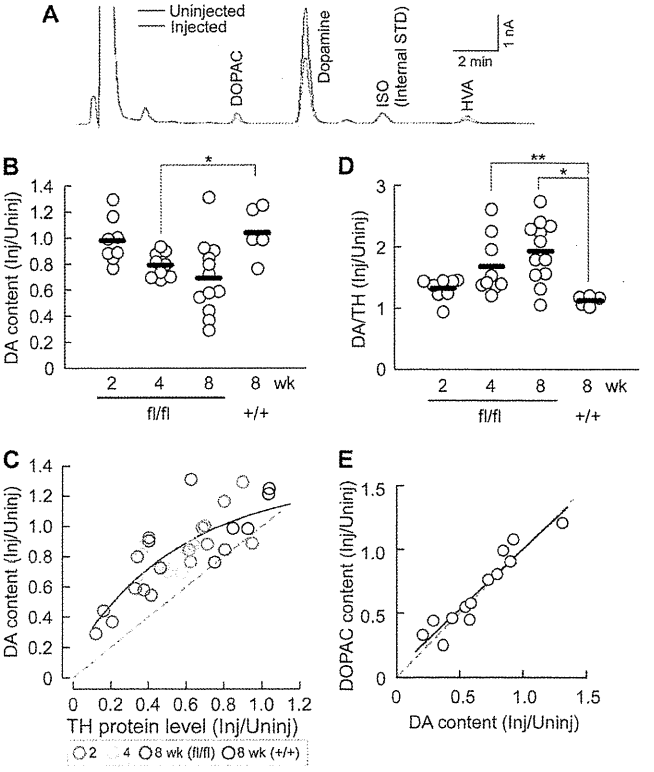

FIGURE 4. **The tissue dopamine contents are better maintained than TH protein levels in the striatum.** *A*, representative chromatograms of the monoamine assay with the homogenates from the uninjected and injected side striata from a $Th^{fl/fl}$ mouse 8 weeks after the injection of AAV-Cre. *B*, summarized DA contents in the striatum after the unilateral AAV-Cre injection to the SNc in the $Th^{fl/fl}$ and $Th^{+/+}$ mice. The monoamine assays were performed using the same extracts used in Fig. 3. The ratios of the dopamine contents in the injected side to the uninjected side are shown. The *open circles* indicate the values from individual animals, and the *bars* indicate the means. n = 8, 9, 12, and 5 brains for 2, 4, and 8 weeks ($Th^{fl/fl}$ mice) and 8 weeks ($Th^{+/+}$ mice) after the injection, respectively. *, $p < 0.05$, Steel's test. The mean dopamine contents in the uninjected side striata were 147.2 ± 10.2 and 158.1 ± 6.7 pmol/mg protein for $Th^{fl/fl}$ and $Th^{+/+}$ mice, respectively at 8 weeks (Steel's test, $p = 0.86$). *C*, the relationship between dopamine contents and TH protein levels. The *circles* represent data from individual animals and are *color-coded* by weeks after the AAV-Cre injection as indicated. The *dotted line* has a slope of 1. The *solid line* indicates an exponential curve fitting. The *points above* the *dotted line* suggest a higher dopamine level per TH protein level in the injected side compared with the uninjected side. *D*, ratio of the dopamine content to the TH protein level normalized to the uninjected side. n = 8, 9, 12, and 5 brains for 2, 4, and 8 weeks ($Th^{fl/fl}$ mice) and 8 weeks ($Th^{+/+}$ mice) after the injection, respectively. We excluded one outlier that showed very low TH protein levels and a high DA/TH ratio (29.8) from the 8-week $Th^{fl/fl}$ group. *, $p < 0.05$; **, $p < 0.01$, Steel's test. *E*, the relationship between DOPAC and dopamine contents in the $Th^{fl/fl}$ mice 8 weeks after the AAV-Cre injection. The data indicate the ratio of the DOPAC contents in the AAV-Cre-injected side of the striatum normalized to the uninjected side. The *open circles* indicate individual data. The *dotted line* has a slope of 1, and the *solid line* indicates a linear fitting. n = 13 mice. Spearman's rank correlation, $p < 0.0001$, $\rho = 0.96$ for DOPAC *versus* dopamine.

mice, respectively, compared with the $Th^{+/+}$ mice at 8 weeks; Fig. 4*B*). Notably, these reductions of dopamine contents were not as striking as those of TH protein levels (Fig. 2*C*). To evaluate the relationship between dopamine and TH, we plotted dopamine contents against TH protein levels (Fig. 4*C*). We found that dopamine contents were less affected than the TH protein levels, and the relationship was fitted well with an exponential curve ($\chi^2 = 0.7391$). The dopamine contents did not show a remarkable reduction until the TH protein levels were decreased by around 50%. Accordingly, the ratios of dopamine contents to TH protein levels were increased, with ratios of 1.32, 1.68, and 1.93 at 2, 4, and 8 weeks after the AAV-Cre injection, respectively, in the $Th^{fl/fl}$ mice, whereas it remained 1.1 in the $Th^{+/+}$ mice at 8 weeks (Steel's test, $p = 0.0665$, 0.0071, and 0.0157 for 2, 4, and 8 weeks for the $Th^{fl/fl}$ mice, respectively, compared with the $Th^{+/+}$ mice at 8 weeks; Fig. 4*D*).

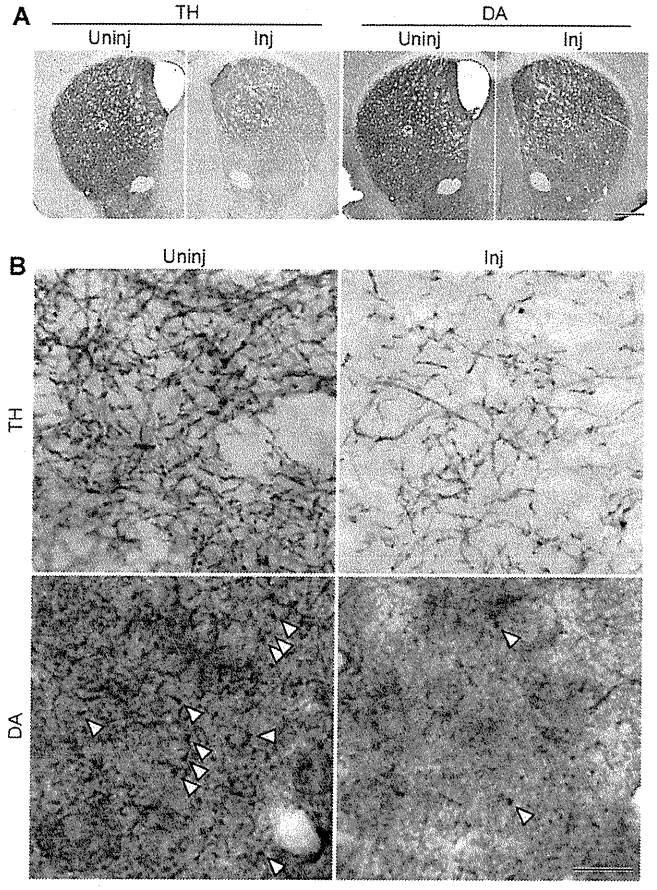

FIGURE 5. **TH and dopamine distribution in the striatum.** *A*, immunohistochemical detection of the striatal TH and DA in the striatum of the $Th^{fl/fl}$ mouse. The mice were fixed with glutaraldehyde 8 weeks after the injection of AAV-GFP/Cre, and the slices cut with a vibratome were stained with antibodies against TH or dopamine. Note that the TH signal in the injected side (*Inj*) was decreased compared with the uninjected side (*Uninj*), whereas the DA signal was less affected. *B*, magnification images of the regions indicated by *asterisks* in *A*, showing TH-expressing axon fibers and dopamine-containing axonal boutons. *Arrowheads* indicate representative puncta of the dopamine signals. *Scale bars*, 0.5 mm (*A*) and 10 μm (*B*).

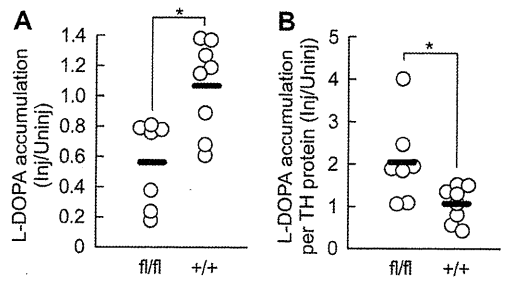

FIGURE 6. **Enhanced *in vivo* L-DOPA synthesis activity per TH protein level.** L-DOPA synthesis activities per TH protein level were estimated by measuring L-DOPA accumulation after *in vivo* administration of NSD-1015, an AADC inhibitor. Striatal homogenates were prepared 30 min after NSD-1015 administration (100 mg/kg, intraperitoneally). L-DOPA levels were measured by HPLC, and TH protein levels were assayed by Western blot. The mice were examined 8 weeks after the AAV-Cre injection. *A*, summary of L-DOPA accumulation in $Th^{fl/fl}$ and $Th^{+/+}$ mice. Data are shown as L-DOPA level in the injected side normalized by the uninjected side. The *open circles* indicate the values from individual animals, and the *bars* indicate the means. The mean L-DOPA level in the uninjected side of the $Th^{+/+}$ mice was 42.1 ± 7.3 pmol/mg protein. *B*, summary of L-DOPA accumulation normalized to the TH protein levels examined by Western blot, providing apparent L-DOPA synthesis activity per TH protein level. *, $p < 0.05$, Mann-Whitney *U* test.

It is known that unilateral depletion of dopamine in the rodent nigra induces ipsilateral rotation behavior in response to reagents enhancing dopaminergic transmission (25, 26). Consistently, $Th^{fl/fl}$ mice with severe unilateral dopamine depletion showed ipsilateral rotation behavior when administered with GBR12909, a potent DAT inhibitor (supplemental Fig. 2*B*), demonstrating the validity of our genetic manipulation to disrupt nigrostriatal dopaminergic transmission.

To further examine the tissue level alterations in the dopamine distribution, we used immunohistochemistry to determine the expression pattern for dopamine and TH in the striatum 8 weeks after the AAV-Cre injection. The mice were fixed transcardially with glutaraldehyde, and the striatal slices were stained with an antibody raised against dopamine-glutaraldehyde conjugate. We used immunoenzyme detection instead of immunofluorescence detection, because glutaraldehyde fixation causes a high fluorescence background. At a lower magnification, TH immunoreactivity was clearly reduced in the AAV-Cre-injected side of the $Th^{fl/fl}$ mice, whereas the dopamine immunoreactivity was only moderately reduced (Fig. 5*A*). These data are consistent with Western blot and monoamine assay results. Higher magnification views showed a reduction in the number of TH-expressing axon fibers in the AAV-Cre-injected side of the $Th^{fl/fl}$ mice (Fig. 5*B*) as observed by immunofluorescence staining (Fig. 3*D*). Moreover, the number of punctate signals of dopamine was also greatly decreased (Fig. 5*B*), suggesting that dopamine levels in the TH-lost axons were substantially reduced. Collectively, these data indicate a compensatory regulation of dopamine levels for a decrease in the TH protein levels. Because TH expression remained in only a subset of dopaminergic axons, these data raise the possibility that a decrease in dopamine synthesis induces a compensatory up-regulation of dopamine synthesis and/or storage in other axons.

Mechanisms of Dopamine Maintenance against TH Protein Loss—The homeostatic compensation of dopamine levels may accompany either an increase in the synthesis of dopamine or a decrease in the degradation of dopamine. To examine the degradation rate of dopamine, we measured the contents of 3,4-dihydroxyphenylacetic acid (DOPAC) and homovanillic acid (HVA), the two major metabolites of dopamine. Reductions of DOPAC and HVA contents were well correlated with that of dopamine in the $Th^{fl/fl}$ mice (Fig. 4*E*). Comparison between injected and uninjected sides showed no difference in the ratio of DOPAC to dopamine (DA) (injected side, 0.12 ± 0.02; uninjected side, 0.15 ± 0.03; Wilcoxon's signed rank test, $p = 0.16$) and in the ratio of HVA to dopamine (injected side, 0.13 ± 0.01; uninjected side, 0.14 ± 0.01; Wilcoxon's signed rank test, $p = 0.43$; supplemental Fig. 3). These data suggest that the degradation rate of dopamine was not significantly changed.

To explore a possible change in the activity of dopamine synthesis pathway, we evaluated *in vivo* L-DOPA synthesis activity by measuring L-DOPA accumulation 30 min after administration of NSD-1015, an AADC inhibitor, 8 weeks after the AAV-Cre injection. We found that the L-DOPA accumulation in the injected side of the striatum was significantly lower in the $Th^{fl/fl}$ mice compared with the $Th^{+/+}$ mice (Mann-Whitney *U* test, $p = 0.0206$; Fig. 6*A*). We then estimated the apparent L-DOPA

synthesis activity per TH protein by normalizing the L-DOPA accumulation with TH protein levels estimated by Western blot analysis. We found that the L-DOPA accumulation per TH protein in the injected side striatum was significantly higher in the $Th^{fl/fl}$ mice than in the $Th^{+/+}$ mice (Mann-Whitney *U* test, $p = 0.0279$; Fig. 6*B*). Considering that L-DOPA is mostly synthesized by TH (14), and the TH proteins remained to be expressed in only a subset of axons, these data suggest that dopamine synthesis activity in the remaining TH-positive axons was augmented to compensate for dopamine level.

Further, we examined if TH phosphorylation at Ser-31 and Ser-40 (27), the two major phosphorylation sites for TH activation, was elevated. However, we did not find a significant change in the phosphorylation states of these Ser residues by Western blot (supplemental Fig. 4). We also measured the contents of biopterin, an essential cofactor for TH, but the contents were not significantly different between the injected and uninjected side (uninjected side, 6.72 ± 0.54 pmol/mg protein; injected side, 6.64 ± 0.49 pmol/mg protein; Mann Whitney *U* test, $p = 0.95$). Thus, the long term up-regulation of L-DOPA synthesis activity may be supported by other molecular mechanisms (*e.g.* a relief of the feedback inhibition of TH by dopamine as a consequence of impaired dopamine synthesis).

In axon terminals, synthesized dopamine is primarily stored in synaptic vesicles, and released dopamine is partly recycled by DAT. When the number of TH-expressing axons was greatly reduced, the manner of dopamine storage could be changed for adaptation. In this context, we examined the level of two major dopamine transporters: vMAT2 and DAT. Western blot analysis showed no significant change in the vMAT2 and DAT protein levels in the injected side striatum compared with the uninjected side in the $Th^{fl/fl}$ mice, despite the great reduction of TH protein levels (supplemental Fig. 5). These data suggest that the numbers of dopaminergic synaptic vesicles and terminals were not grossly altered. Instead, because the majority of dopaminergic axons do not contain normal level of dopamine (Fig. 5*B*), despite the moderate decrease in tissue dopamine contents (Fig. 4), the vesicular dopamine contents in the TH-expressing axons may be increased, and/or TH-negative axons may uptake and contain low level dopamine.

DISCUSSION

Selective Loss of TH Protein in a Subset of Dopaminergic Neurons without Neuronal Degeneration—We took advantage of the Cre-*loxP* system in mice, which enabled us to selectively ablate the *Th* gene and block dopamine synthesis in adult brains. TH expression in the SNc was lost in a subset of SNc dopaminergic neurons by as early as 2 weeks after the AAV-Cre injection. The TH protein level and the number of TH-expressing axons in the striatum were clearly reduced 8 weeks after the AAV-Cre injection. Severe dopamine deficiency accompanied ipsilateral rotation behavior when stimulated with the DAT inhibitor, GBR12909, confirming the integrity of our genetic method to disrupt nigrostriatal dopaminergic transmission.

In contrast, the AADC protein levels and immunohistochemical signals in the striatum and SNc were unaffected 8 or 16 weeks after the AAV-Cre injection. These data suggest that the SNc dopaminergic neurons and axons were mostly preserved for several months without synthesizing dopamine. This is in contrast to neurodegenerative models using neurotoxins, such as 1-methyl-4-phenyl-1,2,3,6-tetrahydropyridine and 6-hydroxydopamine (6-OHDA), which could cause loss of axons and unpredictable side effects. Therefore, our experimental system provides a new animal model of chronic dopamine deficiency in adult brains without neuronal degeneration.

Differential Regulation of TH Protein Level in the Axon Terminals from Soma—Using this *Th* gene ablation strategy in adult brains, we noticed that the decline in the TH protein in the striatum was slower than the reduction of TH-expressing neurons in the SNc (Figs. 2*C* and 3*B*). By direct comparison of TH protein reduction in the striatum and ventral midbrain with Western blotting, we found that the TH protein reduction occurred in a delay, whereas the decay time constants were similar (Fig. 3*C*). This considerable delay of TH protein loss in the striatum suggests a mechanism that maintains the axonal TH protein level for a week or two without *Th* gene transcription. How does such a delay occur?

First, the turnover of TH proteins in axon terminals in the striatum may be slower than that in cell bodies in SNc. In cultured chromaffin cells, the steady-state half-life of the TH protein is about 1 day (28), but it could become longer than 10 days by treatment with translational inhibitors (29). Moreover, incubation with transcriptional inhibitors for 3 days caused no significant loss of the TH protein, although 90% of the TH mRNA was lost (29). Axonal translation may be involved for such a prolonged delay of protein degradation (30, 31). Thus, the difference in TH protein turnover in axon terminals and cell bodies located in SNc may be supported by those multiple regulatory mechanisms.

In addition, the delayed reduction of TH proteins may be attributable to slow axonal transport of TH proteins from soma to axons. Although the mechanism underlying axonal TH transport is not fully understood, the projection from SNc to the striatum in mice is about 2–10 mm, depending on axonal branching (22, 23). The axonal transport of TH was reported to be about 2 mm/h in chicken sciatic nerves (32), but it could be different in the brain because the cytosolic proteins are delivered by the slow axonal transport system at 0.1–8 mm/day (33, 34). These reports raise a possibility that it takes a week or more to transport TH proteins from a soma to axon terminals in the mouse nigrostriatal projection.

Regulation of Dopamine Levels by TH Protein Level and Activity in the Striatum—By quantitative comparison of dopamine contents with TH protein levels in the same striatal tissues, we found that dopamine contents were not simply determined by the TH protein level only. Notably, even 50% loss of TH protein did not remarkably change the dopamine contents. Eight weeks after the AAV-Cre injection, the TH protein levels were reduced to 39%, on average, whereas the dopamine contents were reduced to 69%. Immunohistochemical data showed a similar trend of difference. This finding is consistent with a previous report that dopamine contents in the brain of the adult $Th^{+/-}$ heterozygous mice are normally maintained despite a significant decrease in TH activity (12). Thus, these data indicate that the dopamine levels were primarily determined by TH